nature physics
SUPPLEMENTARY INFORMATION
https://doi.org/10.1038/s41567-018-0313-7
In the format provided by the authors and unedited.

A photon–photon quantum gate based on Rydberg interactions

Daniel Tiarks, Steffen Schmidt-Eberle, Thomas Stolz, Gerhard Rempe and Stephan Dürr*

Max-Planck-Institut für Quantenoptik, Garching, Germany. *e-mail: stephan.duerr@mpq.mpg.de

Supplementary Information:
A Photon-Photon Quantum Gate Based on Rydberg Interactions

Contents

I. EXPERIMENTAL ASPECTS

A. Dipole Trap and Atomic Ensemble

The atomic gas is trapped in an optical dipole trap, similar to Ref. [1]. A light beam at a wavelength of 1064 nm propagates horizontally along the z axis and provides radial confinement with a measured radial trapping frequency of 100 Hz and negligible axial confinement with an estimated trapping frequency of typically 0.1 Hz. With a temperature of typically 0.6 μK, the atomic ensemble is cigar shaped with a Gaussian density profile in the radial direction with an estimated root-mean-square (rms) radius of $\sigma_r = 12$ μm. The EIT coupling light fields at 480 nm create repulsive potentials for the ground-state atoms. These potentials have negligible effect because they are pulsed on with a low duty cycle, as e.g. in Ref. [1]. The atomic ensemble is located in a glass cell with the nearest glass surfaces at a distance of 15 mm from the atoms. No measures have been taken to control the electric field at the position of the atoms.

Two light sheets at a wavelength of 532 nm provide a box-like longitudinal potential. In contrast to Ref. [1], these light sheets have an elliptically shaped spot with waists ($1/e^2$ radii of intensity) of 15 μm along the horizontal z axis and 43 μm vertically and are operated at a power of 0.3 W each. The centers of the plug beams are separated by typically $\Delta z = 100$ μm. The resulting axial density profile is approximately homogeneous with an estimated full width at half maximum (FWHM) of typically $L = 60$ μm. With an atom number of typically 1.3×10^5, we estimate an atomic peak density of typically $\varrho = 2.4 \times 10^{12}$ cm^{-3}. A magnetic field of 14 μT is applied along the symmetry axis of the dipole trap to stabilise the orientation of the atomic spins.

B. Signal and Coupling Light for EIT

Rydberg EIT is created using the 780-nm signal beam (red in Fig. 2) together with Rydberg coupling light. One Rydberg coupling beam at 480 nm (blue in Fig. 2) counterpropagates the signal beam. It is used to store and retrieve the $|L\rangle$ polarisation of the control pulse. The other Rydberg coupling beam at 480 nm (also blue in Fig. 2) copropagates with the signal beam. It is used to create detuned Rydberg EIT for the $|L\rangle$ polarisation of the target pulse. Both Rydberg coupling beams are overlapped with and separated from the EIT signal beam using dichroic mirrors. The Rydberg coupling beams have powers of typically $P_{L,c} = 140$ mW and $P_{L,t} = 26$ mW. Their waists of $w_{L,c} = 21$ μm and $w_{L,t} = 12$ μm are both large compared to the waist of the EIT signal beam of $w_s = 8$ μm so that spatial inhomogeneities in the coupling intensities sampled by the signal light are no major concern. From these parameters, we estimate coupling Rabi frequencies of $\Omega_{L,c}/2\pi = 25$ MHz and $\Omega_{L,t}/2\pi = 20$ MHz.

The ground-state coupling light beam (cyan in Fig. 2) required to store and retrieve the $|R\rangle$ polarisation of the control photon propagates perpendicularly to the EIT signal light. It has a waist of $w_g = 64$ μm and a power P_g between 0.8 and 1.6 μW, from which we estimate a coupling Rabi frequency $\Omega_g/2\pi$ between 6 and 8 MHz.

The 780-nm EIT signal light for the control and target pulses comes from the same laser. It is split into two beams to individually manipulate polarisation, timing, frequency, and power of the control and target signal input pulses. The two beams are recombined on a 50:50 non-polarising beam splitter (NPBS). Whenever we quote the input polarisation of a photon, we refer to the polarisation at the point after this recombination, which is just before entering the first interferometer shown in Fig. 2. As the EIT signal light pulses are created from a laser, they have Poissonian photon number statistics. Typical values for the average photon numbers impinging onto the atomic ensemble are 0.33 and 0.50 for the control and target pulse, respectively.

The incoming control signal pulse has the temporal shape of a Gaussian that is cut off in the center. Without cutting, its rms width would be 0.2 μs. The accompanying control coupling light fields at 480 nm and 780 nm are on for 1 μs during storage and for 2 μs during retrieval.

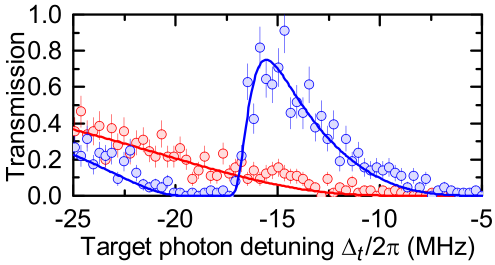

FIG. S1: Target-light Rydberg EIT used for zeroing the conditional optical depth. The transmission of an $|L\rangle$ polarised target photon (blue) exhibits an EIT peak, with a maximum at the two-photon resonance at $\Delta_t/2\pi \sim -15$ MHz. This feature is absent if the target coupling light is switched off (red). The lines show fits of Eq. (S1) to the data. They cross at $\Delta_t/2\pi \sim -17$ MHz. Here, the conditional optical depth ΔOD is approximately zero.

The incoming target signal pulse has a rectangular pulse shape and is 2.6 μs long. The accompanying target coupling light at 480 nm is on for 4.1 μs to leave room for the $\sim$0.4 μs EIT group delay experienced by the target polarisation $|L\rangle$. As the target polarisation $|R\rangle$ does not experience EIT, it acquires negligible group delay. Hence, the longitudinal wave-packet overlap of the target polarisations $|R\rangle$ and $|L\rangle$ deteriorates during propagation through the medium. Hence, in our data analysis of the transmitted target pulse, we include only those typically 2.0 μs in which the target polarisations $|R\rangle$ and $|L\rangle$ overlap well. This reduces the count rate. The coherence time of the incoming target photon is much longer than the EIT group delay so that temporal coherence is not a concern in this differential delay of wave packets.

C. Zeroing the Conditional Optical Depth

As discussed in the Methods Section, zeroing the conditional optical depth ΔOD is important for achieving a high post-selected fidelity of the gate. At a given value of the target coupling detuning, we use the target signal detuning Δ_t to tune ΔOD to zero. Fine tuning Δ_t based on data post-selected upon detection of one control and one target photon would be quite time consuming. As an approximate but much faster method, we consider Fig. S1, which compares the target transmission with and without the target coupling laser, both recorded without sending a control photon into the system. Hence, no post-selection upon a retrieved control photon is needed and the data acquisition rate is much higher.

To understand, why Fig. S1 helps finding the two-photon detuning for which $\Delta OD = 0$, we consider the step-function approximation discussed in section II B. It suggest that in Fig. S1, the blue and red data can be regarded as measures for $\mathrm{Im}\,\chi_u$ and $\mathrm{Im}\,\chi_b$, where χ_u and χ_b denote the susceptibility in the unblocked and blocked volume, respectively. In this approximation, $\Delta OD = 0$ is obtained for that value of Δ_t where the two lines in Fig. S1 cross.

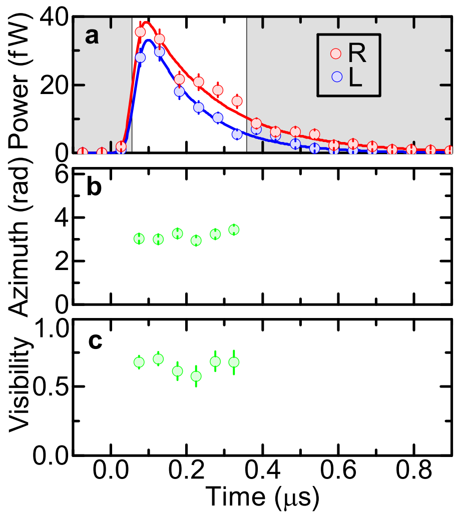

FIG. S2: Performance of the quantum memory for the control qubit. **a** The retrieved power is well balanced between $|R\rangle$ and $|L\rangle$ at all times. **b**, **c** Azimuth and visibility of the retrieved light depend hardly on time. The visibility is high.

D. Quantum Memory

The retrieval efficiency from the Rydberg state exhibits damped oscillations as a function of the dark time [2, 3]. For the parameters of our experiment, the first revival of the efficiency occurs at a dark time of 4.5 μs, which is why we choose this value for the dark time.

To characterise the quantum memory, we perform single-photon polarisation tomography of the retrieved light. The normalised single-photon Stokes parameters are $S_i = (P_i - P_{i^\perp})/(P_i + P_{i^\perp})$, where $i \in \{H, D, R\}$ denotes horizontal, diagonal (45°), and righthanded circular polarisation, P_i the power behind a polariser which transmits the polarisation i, and $H^\perp = V$, $D^\perp = A$, and $R^\perp = L$ denote vertical, anti-diagonal (-45°), and left-handed circular polarisation. The visibility, also known as the degree of (maximum) linear polarisation, is $V = (S_H^2 + S_D^2)^{1/2}$. The azimuth φ is defined modulo 2π by $S_H = V\cos\varphi$ and $S_D = V\sin\varphi$. For $S_R = 0$, V is a measure for how much coherence there is between the $|R\rangle$ and $|L\rangle$ polarisations. We denote the visibilities of the control and target qubits as V_c and V_t, respectively.

For an $|R\rangle$ polarised input, the retrieved light is found to have a fraction $\epsilon_R = 4.8(5)\%$ of its energy in $|L\rangle$. Likewise, for an $|L\rangle$ polarised input we obtain $\epsilon_L = 2.5(6)\%$ in $|R\rangle$. Hence, the two polarisations $|R\rangle$ and $|L\rangle$ are well maintained during storage. To test how well coherence between $|R\rangle$ and $|L\rangle$ is maintained, we choose an input superposition such that the $|R\rangle$ and $|L\rangle$ components of the output energy are fairly well balanced. The results of this measurement are shown in Fig. S2. Fig. S2a shows that the retrieved light powers in $|R\rangle$ and $|L\rangle$ are fairly well balanced at all relevant times. To minimise the influence of detector dark counts, we analyse data only in the unshaded region. Polarisation tomography yields the azimuth φ and the visibility V_c. These quantities, shown in Figs. S2b and c, are to a good approximation time independent, which is advantageous because it implies that we can effortlessly average data over the full data analysis time window. This averaging yields $V_c = 0.66(2)$. The average fidelity of the quantum memory is $F_m = (2 + 2V_c + (1 + \epsilon_R)^{-1} + (1 + \epsilon_L)^{-1})/6 = 0.875(7)$, post-selected upon detection of the target photon. For comparison, if light is sent through both interferometers in the absence of atoms, we measure $V = 0.97$ for an appropriate input state. Hence, V_c is predominantly limited by the atomic memory, not by the interferometers. The measured value of the post-selected average fidelity clearly exceeds the classical limit of 2/3.

Various effects can limit the visibility V_c achievable in the control qubit after retrieval from the ground and Rydberg state. This is because the phase of the retrieved light depends on the relative phase accumulated during the dark time between an atomic superposition and a local oscillator, somewhat like in Ramsey spectroscopy. But in contrast to normal Ramsey spectroscopy, here three local oscillators instead of one contribute, namely the ground-state coupling laser at 780 nm, the control Rydberg coupling laser at 480 nm, and the rf reference oscillator, which drives the PLLs in both interferometers. The large wavelength difference between these two lasers makes it difficult to achieve low relative phase noise between them. The very different principal quantum numbers of the atomic states result in large differential electric polarisabilities for static or dynamic electric fields. Overall, various effects contribute to phase fluctuations, e.g. phase fluctuations of both control coupling lasers, fluctuating Zeeman and Stark effects in the presence of fluctuating magnetic and electric fields, fluctuating differential light shifts in the presence of power fluctuations in the dipole trapping light and in the target coupling light, and a distribution of differential light shifts in the dipole trapping light and in the target coupling light resulting from the thermal position distribution of the atoms. Clearly, the large number of possible issues listed here offers room for future improvements.

Reaching well-balanced powers of the $|R\rangle$ and $|L\rangle$ polarisations in the retrieved light at all relevant times is nontrivial. First, the time scales at which the retrieved powers decay in Fig. S2a must be made independent of the polarisation. We achieve this by adjusting the ratio of the intensities of the two control coupling light fields. Second, the overall retrieved energies, i.e. the areas under the curves in Fig. S2a, must be made independent of the polarisation. We reach that by adjusting the input polarisation. A possible differential group delay between the retrieved $|R\rangle$ and $|L\rangle$ polarisations could, in principle, be removed by delaying one of the retrieval coupling pulses, but this is not needed in our experiment.

Likewise, reaching a time-independent value of the azimuth in Fig. S2b is nontrivial. Under general conditions we typically observe some linear slope in Fig. S2b. However, after tuning the frequency of the control coupling laser to achieve $\beta_{c,L} - \beta_{c,R} = 0$ for all dark times, as discussed in the Methods Section, the linear slope in Fig. S2b vanishes automatically.

E. Count Rates

The combined efficiencies for storage and retrieval of the control qubit for a dark time of $t_d = 4.5$ μs in the presence of a target pulse are roughly $\eta_R \sim 10\%$ and $\eta_L \sim 3\%$ for the $|R\rangle$ and $|L\rangle$ polarisations, respectively. The transmission of an $|R\rangle$ polarised target qubit is $T_R = e^{-OD_R} \sim 77\%$. The transmission of an $|L\rangle$ polarised target qubit is roughly $T_L \sim 15\%$, in reasonable agreement with the transmission at the point, where the two lines in Fig. S1 cross. This yields an efficiency $\eta_i T_j$ between 8% and 0.5% that a photon pair impinging onto the atomic ensemble is transmitted by the atomic ensemble, depending on the input polarisations $i, j \in \{R, L\}$. Note that future improvements regarding these numbers are possible.

Let P_{shot} denote the probability of a coincidence detection of one control and one target photon in a single experimental shot, which consists of storage of a control photon, propagation of a target photon, and retrieval of the control photon. In addition to the above-discussed efficiency $\eta_i T_j$ of the gate, several technical issues contribute to P_{shot}, namely the quantum efficiency of 0.5 of each avalanche photodiode (APD) used for detection, the probability that an incoming pulse contains zero photons in a given shot, the non-unity transmission through the second interferometer, and the non-unity transmission through two single-mode optical fibres, one of which is located right after the atomic ensemble, the other right after the second interferometer. However, photon loss in components in front of the atomic ensemble is easily compensated by increasing the input power, as discussed in the Methods Section.

In daily alignment, we typically measure $P_{\text{shot}} = 1.3 \times 10^{-5}$ for the entangling-gate operation. Such an experimental shot is repeated every 100 μs as in Ref. [1]. The illumination with light causes spontaneous emissions which result in loss of atoms by spontaneous evaporation from the shallow dipole trap. To avoid a noticeable drop in atom number, we perform only 10^4 experimental shots and then prepare a new atomic ensemble. A new atomic sample is prepared every 18 s so that in one minute, we detect an average number of 0.4 coincidences.

II. MODELLING DETAILS

A. Rydberg EIT

The linear electric susceptibility χ for Rydberg EIT in a ladder-type atomic level scheme with signal transition $|g\rangle \leftrightarrow |e\rangle$ and coupling transition $|e\rangle \leftrightarrow |r\rangle$ can be modelled as, see e.g. Ref. [1]

$$\chi = i\chi_0\Gamma_e \left(\Gamma_e - 2i\Delta_s + \frac{|\Omega_c|^2}{\gamma_{rg} - 2i(\Delta_c + \Delta_s)}\right)^{-1}, \quad \text{(S1)}$$

where $\Gamma_e = 1/(26 \text{ ns})$ is the population decay rate of the intermediate state $|e\rangle$, γ_{rg} is the dephasing rate between states $|g\rangle$ and $|r\rangle$, Ω_c is the Rabi frequency on the coupling transition, $\Delta_s = \omega_s - \omega_{s,\text{res}}$ and $\Delta_c = \omega_c - \omega_{c,\text{res}}$ are the single-photon detunings of signal and coupling light, respectively, and $\chi_0 = 2\varrho|d_{ge}|^2/\epsilon_0\hbar\Gamma_e$ is the value of $|\chi|$ for $\Omega_c = \Delta_s = 0$, where ϵ_0 is the vacuum permittivity, d_{ge} the electric dipole moment for the signal transition, and ϱ the atomic density. Propagation through a homogeneous medium of length L multiplies the complex amplitude $\boldsymbol{E}_0(z)$ of the electric field $\boldsymbol{E}(z,t) = \frac{1}{2}\boldsymbol{E}_0(z)e^{-i\omega_s(t-z/c)}$+c.c. of the light by a factor $e^{-OD/2+i\beta}$ with the optical depth $OD = k_s L \,\text{Im}(\chi)$ and the phase shift $\beta = k_s L \,\text{Re}(\chi)/2$, where $k_s = \omega_s/c$ is the vacuum wave vector of the signal light and c the vacuum speed of light. According to Eq. (S1), the optical depth reaches its maximum $OD_\text{max} = k_s L \chi_0$ for $\Omega_c = \Delta_s = 0$.

The parameters of the atomic ensemble listed in section I A can be used to calculate OD_max. A simple calculation in the limit of vanishing waist of the signal beam $w_s \to 0$ yields a value of typically $OD_\text{max} \sim 40$.

The fit of Eq. (S1) to the target-light EIT data (blue) in Fig. S1 yields a coupling Rabi frequency of $\Omega_{L,t}/2\pi = 12.5(3)$ MHz for the target light, in reasonable agreement with the above estimate, and a dephasing rate of $\gamma_{rg} = 1.2(3)\ \mu\text{s}^{-1}$, similar to the value obtained in Ref. [1]. Dephasing is implemented in the model as a Markovian process described by $\partial_t\rho_{rg} = -\frac{1}{2}\gamma_{rg}\rho_{rg}$, as in Ref. [4]. Here, ρ is the density matrix. In the absence of additional driving terms, this would produce an exponential temporal decay of ρ_{rg}. This makes it easy to implement the dephasing in an analytical calculation but it is not guaranteed to give an accurate description. For example, when applying this ansatz to describe the retrieval efficiency as a function of dark time, a simple model predicts an exponential decay of the efficiency with a $1/e$ time of $1/\gamma_{rg}$. As discussed in section I D, we observe damped oscillations instead. This shows that the Markovian ansatz does not capture all the relevant physical effects. From this perspective, γ_{rg} represents a lowest-order approximation of the dephasing. Hence, when making large changes to other parameters, such as Ω_c or the atomic density ϱ, there is no guarantee that γ_{rg} remains unchanged. On the other hand, γ_{rg} is useful for modelling because it gives analytic curves which fit well to the transmission and phase shift as a function of Δ_s, see e.g. Fig. S1 or Ref. [1].

B. Rydberg Blockade

The presence of a stored control excitation in the Rydberg state $|69S\rangle$ creates a van der Waals energy $V(r) = -C_6/r^6$ for the propagating Rydberg polariton of the target polarisation $|L\rangle$, where r is the distance between the two excitations and C_6 the van der Waals coefficient. For the combination of Rydberg states $|67S, F{=}m_F{=}2\rangle$ and $|69S, F{=}m_F{=}2\rangle$ in ^{87}Rb, quantum defect theory yields $C_6 = 2.3 \times 10^{23}$ a.u. [5], where one atomic unit (a.u.) equals 9.573×10^{-80} Jm^6. The van der Waals potential effectively modifies $\omega_{c,\text{res}}$ and, hence, the target coupling detuning according to $\Delta_c(r) = \Delta_{c,u} - V(r)/\hbar$, where $\Delta_{c,u}$ is the unblocked value. This creates a corresponding r dependence of χ according to Eq. (S1). Obviously $\Delta_c(r)$ diverges for $r \to 0$. χ, however, approaches a finite value, which we call the completely blocked value $\chi_b = \lim_{r\to 0}\chi(r)$. This value could alternatively be obtained by switching the EIT coupling light off. Hence, it equals the response of the two-level atom $|g\rangle \leftrightarrow |e\rangle$. We denote the unblocked value as $\chi_u = \lim_{r\to\infty}\chi(r)$.

Inspection of $\text{Re}\,\chi(r)$ for the parameters of our experiment shows that $\text{Re}\,\chi(r)$ is well approximated by a step function. We define the blockade radius r_b as the value of r at which $\text{Re}\,\chi$ reaches the arithmetic mean of its unblocked value and its completely blocked value $\text{Re}[\chi(r_b)] = \frac{1}{2}\text{Re}(\chi_b + \chi_u)$. The step-function approximation sets $\text{Re}\,\chi = \text{Re}\,\chi_u$ for $r > r_b$ and $\text{Re}\,\chi = \text{Re}\,\chi_b$ otherwise. An analogous argument applied to $\text{Im}\,\chi(r)$ yields a blockade radius $r_{b,i}$ defined by $\text{Im}[\chi(r_{b,i})] = \frac{1}{2}\text{Im}(\chi_b + \chi_u)$ and a step-function approximation $\text{Im}\,\chi = \text{Im}\,\chi_u$ for $r > r_{b,i}$ and $\text{Im}\,\chi = \text{Im}\,\chi_b$ otherwise. Typically $r_{b,i} \sim r_b$. To illustrate this, we temporarily consider the simple example of zero dephasing $\gamma_{rg} = 0$, large single-photon detuning $|\Delta_s| \gg \Gamma_e$, and zero two-photon detuning $\Delta_{c,u} + \Delta_s = 0$. Here, one obtains the analytic results $r_b = |4C_6\Delta_s/\hbar\Omega_c^2|^{1/6}$ (see also Ref. [6]) and $r_b/r_{b,i} = (1+\sqrt{2})^{1/6} \sim 1.16$.

In our experiment, Rydberg blockade manifests itself in the conditional optical depth ΔOD and the conditional phase shift $\Delta\beta$. Suppressing fluctuations in ΔOD and $\Delta\beta$ is important for avoiding decay of coherence between the $|L\rangle$ and $|R\rangle$ polarisations of the target qubit in the presence of a stored Rydberg excitation. As the Rydberg blockade radius of $r_b = 16\ \mu$m (see section II C) is much larger than the EIT signal beam waist of $w_s = 8$ μm, the transverse degrees of freedom within the signal beam are irrelevant for the Rydberg blockade. This produces an effectively one-dimensional (1D) situation, in which fluctuations in ΔOD and $\Delta\beta$ otherwise caused by different relative transverse positions of the control and target photons are suppressed. In addition, the medium is to a good approximation homogeneous in the longitudinal direction and the transverse size of the medium

$\sigma_r = 12\ \mu$m is much larger than the $w_s = 8\ \mu$m EIT signal beam waist. This suppresses fluctuations in ΔOD and $\Delta\beta$ otherwise caused by storage of the control photon at positions with different atomic densities.

The conditional optical depth ΔOD and the conditional phase shift $\Delta\beta$ are defined as the difference between the values obtained in the presence and in the absence of a stored Rydberg excitation. We consider a 1D model, in which the signal beam propagates along the z axis, assume that the medium is homogeneous and extends from $z = 0$ to $z = L$, use the step-function approximation, denote the position of the stored control excitation as z_s, and introduce $L_b = \min(r_b, z_s) + \min(r_b, L - z_s)$ to denote the length of the blocked volume and a similar expression for $L_{b,i}$. This yields $\Delta OD = k_s L_{b,i} \operatorname{Im}(\chi_b - \chi_u)$, $\Delta\beta = k_s L_b \operatorname{Re}(\chi_b - \chi_u)/2$, and $L_b \leq \min(2r_b, L)$.

C. Choice of Parameter Values

The following simple consideration yields a necessary condition for achieving $|\Delta\beta| = \pi$. From Eq. (S1) one can show that $|\operatorname{Re}(\chi)| \leq \chi_0/2$. This yields the upper bound $|\Delta\beta| \leq k_s L_b \chi_0/2 = OD_b/2$, where we abbreviated the blocked optical depth $OD_b = OD_{\max} L_b/L = k_s L_b \chi_0$. Hence, for reaching $|\Delta\beta| = \pi$ we obtain the necessary condition $OD_b \geq 2\pi$. Note that $|\Delta\beta| \leq OD_b/2$ is a tight bound because it can be reached, at least hypothetically, namely if and only if $\gamma_{rg} = 0$, $|\Delta_s| = \Gamma_e/2$, and $\Delta_{c,u} + \Delta_s = |\Omega_c|^2/8\Delta_s$. It turns out that for these parameters $\Delta OD = 0$, which is good. But at the same time $\operatorname{Im}\chi_b = \operatorname{Im}\chi_u = \chi_0/2$ so that $OD = OD_{\max}/2$. Combination with $L_b \leq L$ shows that the transmission $T = e^{-OD}$ of the target intensity has the upper bound $T \leq e^{-OD_b/2} = e^{-\pi} \sim 0.04$. For $L = 4r_b$, as in our experiment, $L_b \leq 2r_b = L/2$ even yields $T \leq e^{-OD_b} = e^{-2\pi} \sim 2 \times 10^{-3}$.

The problem of this very low target transmission can be mitigated when using parameter values which do not reach the bound $|\Delta\beta| = OD_b/2$. Obviously, this comes at the cost of the need for larger OD_b. A simple estimate is obtained when assuming for simplicity that $\gamma_{rg} = 0$. Hence, the condition $\Delta OD = 0$ yields $\Delta_{c,u} + \Delta_s = |\Omega_c|^2/8\Delta_s$ and $\Delta\beta/OD_b = -2\Delta_s\Gamma_e/(4\Delta_s^2 + \Gamma_e^2)$. Using $\operatorname{Im}\chi_b = \chi_0\Gamma_e^2/(4\Delta_s^2 + \Gamma_e^2)$, one obtains $OD = k_s L \operatorname{Im}\chi_b = -\frac{\Gamma_e}{2\Delta_s}\Delta\beta\frac{L}{L_b}$. When increasing $|\Delta_s|$ at fixed L, L_b, and $\Delta\beta$, the optical depth decreases as $1/|\Delta_s|$. Hence, it is advantageous to work at larger $|\Delta_s|$, which according to the above relation for $\Delta\beta/OD_b$ requires larger OD_b to keep $\Delta\beta$ fixed. In this model the optical depth vanishes for $|\Delta_s| \to \infty$. This is unrealistic because in this limit it becomes crucial that the dephasing rate γ_{rg} is actually nonzero. A more elaborate model optimizing the target transmission while taking $\gamma_{rg} \neq 0$ into account is presented in the rest of this section. For simplicity, this model assumes $L_b = 2r_b$ although this is not necessarily the case, see section II D.

In the Methods Section, we already motivated the choice of several parameters, namely the Rydberg states $|67S\rangle$ and $|69S\rangle$, the transition $|5S_{1/2}, F{=}m_F{=}2\rangle \leftrightarrow |5P_{3/2}, F{=}m_F{=}3\rangle$ for $|L\rangle$ polarised signal light, the atomic density $\varrho \sim 2 \times 10^{12}$ cm^{-3}, and the length of the medium $L \sim 60\ \mu$m. This choice of the atomic levels fixes the parameters $2\pi/k_s = 780.24$ nm, $\Gamma_e/2\pi = 6.07$ MHz, $d_{ge} = 2.54 \times 10^{-29}$ Cm, and $C_6 = 2.3 \times 10^{23}$ a.u. Empirically, we find $\gamma_{rg} \sim 1.2\ \mu\text{s}^{-1}$ for these parameters, see e.g. Fig. S1. In addition, the sign of Δ_s should be chosen such that $C_6\Delta_s < 0$, as discussed e.g. in Ref. [1]. With these parameters, a 1D model with homogeneous atomic density yields $OD_{\max} = 35$.

We have three parameters left to choose, namely $\Delta_{c,u}$, $|\Delta_s|$, and $|\Omega_c|$. We wish to satisfy two constraints $\Delta\beta = \pi$ and $\Delta OD = 0$. With three independent parameters and two constraints, there is one degree of freedom left to choose. We decide to use this degree of freedom to minimize the optical depth. As we use the step-function approximation, we have $\Delta OD = 2k_s r_{b,i} \operatorname{Im}(\chi_b - \chi_u)$. Hence, the constraint $\Delta OD = 0$ implies $\operatorname{Im}(\chi_u) = \operatorname{Im}(\chi_b)$ so that minimizing $\operatorname{Im}(\chi_u)$ or minimizing $\operatorname{Im}(\chi_b)$ is equivalent. Therefore we do not need to make a choice which of the two we want to minimize. The constraint $\Delta OD = 0$ also implies that $r_{b,i}$ disappears from the problem.

The constraint $\Delta OD = 0$ can be solved analytically to yield $\Delta_{c,u} = -\Delta_s + [|\Omega_c|^2\Gamma_e + \gamma_{rg}(-4\Delta_s^2 + \Gamma_e^2)]/8\Gamma_e\Delta_s$. The remaining task is to minimize $\operatorname{Im}(\chi_b)$ with free parameters $|\Delta_s|$ and $|\Omega_c|$ under the constraint $\Delta\beta = \pi$. With some effort this problem can be solved analytically using the method of Lagrange multipliers, yielding $|\Omega_c|^2 = 6\gamma_{rg}(4\Delta_s^2 + \Gamma_e^2)/\Gamma_e$ and $\Delta_s = \frac{1}{2}\Gamma_e(\zeta + \sqrt{\zeta^2 - 1})\operatorname{sgn}(-C_6)$, where $\operatorname{sgn}(x) = x/|x|$ and where we abbreviated a dimensionless parameter $\zeta = (2/7)\,|C_6/\hbar\gamma_{rg}|^{1/7}\,(3\chi_0 k_s/\pi)^{6/7}$. Obviously, a physical solution requires Δ_s to be real, i.e. $\zeta \geq 1$. This puts a nontrivial constraint at the parameters for which the gate can function at all. For the above-listed parameters of our experiment, we obtain $\zeta = 2.6$. As discussed below, reducing ζ would result in lower transmission, which is undesired. If ζ were reduced below unity, it would become impossible to simultaneously achieve $\Delta\beta = \pi$ and $\Delta OD = 0$.

The model suggests that the optimal parameter settings should be $\Delta_s/2\pi = -15$ MHz, $|\Omega_c|/2\pi = 13$ MHz, and a small two-photon detuning $(\Delta_{c,u} + \Delta_s)/2\pi = -1.3$ MHz. We adopt the first two suggestions to a good approximation. The energy of the Rydberg state is not known very accurately in the experiment. Hence, we experimentally fine tune the two-photon detuning to achieve $\Delta OD = 0$.

Moreover, this 1D model predicts $r_b = 16\ \mu$m, $OD_b = 19$, and $\operatorname{Im}(\chi_b) = \operatorname{Im}(\chi_u) = \chi_0\Gamma_e/4\zeta|\Delta_s| = 2.6 \times 10^{-3}$. From the latter, the model predicts a transmission of $e^{-k_s L \operatorname{Im}(\chi_u)} = 0.26$ for the $|L\rangle$ polarisation of the target photon. The value of the transmission, measured where the two lines cross in Fig. S1, is approximately half as large. This deviation comes about because Fig. S1 happened to be measured at $OD_{\max} \sim 55$, which is quite a bit larger than the typical value normally used in our experiment.

For these values, the parameter $\zeta^2 \sim 7$ is large compared to unity. Expanding the above solution in a power series for large ζ yields

$$\begin{aligned}\mathrm{Im}(\chi_b) &= \frac{\chi_0}{4\zeta^2}[1+O(\zeta^{-2})] \\ &= \frac{49}{16}\left(\frac{\pi}{3k_s}\right)^{12/7}\left(\frac{\hbar\gamma_{rg}}{|C_6|}\right)^{2/7}\left(\frac{1}{\chi_0}\right)^{5/7}[1+O(\zeta^{-2})].\end{aligned} \tag{S2}$$

The first equality shows that maximizing ζ is crucial for achieving small $\mathrm{Im}(\chi_b)$. The second equality shows that if future improvements can reduce the dephasing rate γ_{rg}, then $\mathrm{Im}(\chi_b)$ can be reduced. In this model, the hypothetical limit $\gamma_{rg} \to 0$ would result in $|\Delta_s| \to \infty$, $\Omega_c \to 0$, and $\mathrm{Im}(\chi_b) \to 0$, i.e. perfect transmission. The radiative lifetime of the Rydberg state, of course, sets a fundamental lower limit on γ_{rg}. For the $|67S\rangle$ state in a room-temperature environment, this limit is $\gamma_{rg} = 1/(0.14 \text{ ms})$ [5], a factor of $\sim$200 lower than the present best-fit value. There is clearly room for improvements.

This analysis reveals that the dephasing rate γ_{rg} is a crucial performance-limiting element which implies that the laissez-faire attitude with which some proposals neglect dephasing should be reconsidered. On the other hand, our success in demonstrating a gate with our comparatively simple scheme despite the presence of dephasing is clearly an encouraging step for tackling some of the more elaborate proposals for Rydberg-based photon-photon gates. For example, cavity-based proposals [7–9] offer a way to operate at lower atomic density and therefore hopefully lower dephasing without incurring a loss in the multi-pass blocked optical depth. In addition, they can operate on single-photon resonance and use the cavity mirrors to convert conditional absorption into a conditional phase shift. Both aspects promise large margins for improving the performance of the gate.

D. Visibility of the Target Photon

Based on the finite length L of the medium, we will now derive an upper bound on the target-photon visibility V_t achievable in the present scheme. This limit comes about because in our experiment $L > r_b$ so that the length of the blocked volume L_b depends on the position z_s at which the control excitation is stored. As z_s is a random variable, so are L_b and $\Delta\beta$.

We assume that the quantum state of the stored excitation is initially $|u\rangle = \int dz u(z)|z\rangle$ with $\langle u|u\rangle = 1$, where $u(z) = \langle z|u\rangle$ is the spatial wave function. After a target pulse containing a single photon in the input polarisation state $|H\rangle$ propagated through the medium, the two excitations are finally in the state $|\psi\rangle = \frac{1}{\sqrt{2}}\int dz(|R\rangle + e^{i\Delta\beta(z)}|L\rangle)\otimes u(z)|z\rangle$, in which the target-photon polarisations became entangled with the position z of the stored excitation. As we eventually do not measure z, we take the partial trace over this degree of freedom, yielding a reduced density matrix for the target-photon polarisation $\rho_t = \frac{1}{2}[|R\rangle\langle R| + |L\rangle\langle L| + (V_t e^{i\beta_4}|L\rangle\langle R| + \text{H.c.})]$ with parameters $\beta_4 \in]-\pi,\pi]$ and $V_t \geq 0$ defined by

$$V_t e^{i\beta_4} = \int_{-\infty}^{\infty} dz |u(z)|^2 e^{i\Delta\beta(z)}. \tag{S3}$$

V_t is the visibility introduced above. This result is plausible. Averaging $e^{i\Delta\beta(z)}$ over z with weighting function $|u(z)|^2$ yields an effective phase factor with reduced magnitude.

For simplicity, we assume that $|u(z)|^2$ is constant inside the medium and zero outside the medium. A proper handling of the cases resulting from $L_b = \min(r_b, z_s) + \min(r_b, L - z_s)$ yields

$$V_t e^{i\beta_4} = \begin{cases} e^{i\Delta\beta_b}[1 - \frac{2r_b}{L} - \frac{4ir_b}{L\Delta\beta_b}(1 - e^{-i\Delta\beta_b/2})], & 2r_b < L \\ e^{i\Delta\beta_b L/2r_b}[-1 + \frac{2r_b}{L} - \frac{4ir_b}{L\Delta\beta_b}(1 - e^{i\Delta\beta_b(r_b - L)/2r_b})], & r_b < L < 2r_b \\ e^{i\Delta\beta_b L/2r_b}, & L < r_b, \end{cases} \tag{S4}$$

where $\Delta\beta_b = k_s r_b \,\mathrm{Re}(\chi_b - \chi_u)$ denotes the bulk value of $\Delta\beta$ that is obtained for $L \to \infty$ which implies $L_b = 2r_b$. Obviously $V_t = 1$ for $L < r_b$ which is plausible because in this case the stored excitation always blocks the complete medium. In the opposite limit $L \to \infty$, one also obtains $V_t \to 1$ which is plausible because in this case $\Delta\beta(z_s) = \Delta\beta_b$ for almost all z_s.

In our experiment, the measured value of the conditional phase shift is β_4 and we tune the experimental parameters such that this equals π. To model this for a given value of L/r_b, we numerically search the value of $\Delta\beta_b$ which yields $\beta_4 = \pi$ in Eq. (S4). Numerical results for the resulting values of V_t are shown in Fig. S3.

For $L \sim 4r_b$, as in our experiment, Fig. S3 yields $V_t \sim 0.85$. As other experimental imperfections will tend to reduce the measured value of V_t, this value is to be regarded as an upper bound on V_t. In Ref. [1] also with $L \sim 4r_b$, we measured $V_t = 0.75(14)$ which is a bit worse than the upper bound estimated here.

From this perspective, it would seem desirable to work

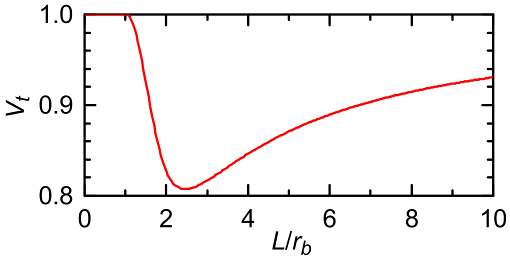

FIG. S3: Expected dependence of the visibility of the target pulse V_t on the length of the medium L in units of the blockade radius r_b. For $L/r_b \leq 1$ the complete medium is blocked, resulting in perfect visibility. For larger L the conditional phase shift depends on the random position z_s at which the control excitation is stored. As z_s is not measured, the visibility is reduced. Parameters in the model are chosen such that the conditional phase shift becomes π after averaging over z_s.

at $L = r_b$ because here this model predicts $V_t = 1$. The problem with this idea is that if the atomic density is kept the same, then ζ would be approximately halved, which would on one hand drastically reduce the target light transmission and on the other hand bring ζ close to unity so that it would be difficult to stably produce $\Delta\beta = \pi$. To avoid these problems, one could approximately double the atomic density but that would increase dephasing issues which would harm efficiency and postselected fidelity. However, if one found a way to reduce the dephasing rate, working at $L = r_b$ would become an appealing option for increasing V_t in the future. In our present experiment we accept a moderate reduction in V_t at this point to avoid the problems arising from increased dephasing.

Alternatively, one could work at much larger L, because $V_t \to 1$ for $L \to \infty$. However, as seen in Fig. S3 a large increase in L would be needed to make a big difference for V_t. With the present experimental imperfections, the resulting reduction in the efficiency would outweigh the benefits from the increase in V_t.

E. Choice of β_2

To motivate the choice $\beta_2 = \pi$, recall that we switch the rf power driving the AOM in the first interferometer to compensate for $OD_1 \neq OD_2$. In principle, we could also switch the phase of the same rf field to compensate for $\beta_1 \neq \beta_2$. As discussed in the Methods Section, the choice to compensate $OD_1 \neq OD_2$ before the photons interact with the atomic ensemble has the advantage that a reduction of count rate can be avoided. As compensating a phase shift does not introduce photon loss, this argument does not apply to the compensation of $\beta_1 \neq \beta_2$. Hence, we can just as well compensate $\beta_1 \neq \beta_2$ after the photons interacted with the atoms, e.g. by switching the phase of the rf field driving the AOM in the second interferometer. However, some technical effort would be required to make switching the phase of one of these rf fields compatible with the PLL used to stabilize that interferometer against drift. Instead, we choose an equivalent method which is technically simpler.

In this context, it comes in handy that for detection, the photons are first sent though a 50:50 NPBS. Each output beam of the NPBS is sent through a set of waveplates for basis selection and then through a PBS. There is a total of four output beams of the two PBSs. Each of them is sent onto an APD. Hence, we could set the waveplates in front of one (the other) PBS to give the required compensation for the control (target) photon. The disadvantage of this method is that the NPBS does not selectively send the photons into the desired paths. Hence, one would lose a factor of four in count rate with this method. In principle, one could overcome this by replacing the NPBS with a device, such as an AOM, which allows it to time-dependently steer the photons into the desired paths.

For $\beta_2 - \beta_1 = \pi$, however, one can stick with the NPBS and use identical waveplate settings in front of both PBSs. This is because for $\beta_2 - \beta_1 = \pi$ the Stokes parameters S_H and S_D of the target photon simply have opposite sign compared to the Stokes parameters of the control photon. This inversion can be compensated after data acquisition during data processing. For the parameters of our experiment, the value of $\beta_2 - \beta_1$ happens to be close to π anyway. By fine tuning an experimental parameter, we can easily make it equal π. As we choose parameters such that $\beta_1 = 0$, this yields $\beta_2 = \pi$.

F. Fidelity of the Entangling-Gate Operation

Fluctuations and nonideal average values in the experimental parameters reduce the fidelity of the entangling-gate operation. Here, we present a simple model of these effects, which yields an upper bound for the fidelity of the entangling-gate operation given the measured visibilities of the control qubit V_c and target qubit V_t. Of course, as soon as one manages to improve the visibilities, the upper bound will improve as well. For simplicity, we assume that nonideal behaviour comes entirely from fluctuations in the phases.

We assume that each realisation of the experiment yields an output state vector in which all of the states $|RR\rangle$, $|RL\rangle$, $|LR\rangle$, and $|LL\rangle$ have equal population. Hence, the output state vector has the general form

$$|\psi_\beta\rangle = \frac{1}{2} e^{i\beta_0} (|RR\rangle + e^{i\beta_2}|RL\rangle + e^{i\beta_1}|LR\rangle + e^{i\beta_1+i\beta_2+i\beta_3}|LL\rangle), \quad \text{(S5)}$$

with four real phases β_0, β_1, β_2, and β_3, the significance of which was discussed in the Methods Section. The input state $|HH\rangle$ for the entangling-gate operation equals $|\psi_\beta\rangle$ with $\beta_1 = \beta_2 = \beta_3 = 0$. The ideal output state $|\psi_i\rangle$ equals $|\psi_\beta\rangle$ with $\beta_1 = 0$ and $\beta_2 = \beta_3 = \pi$. The state

$|\psi_\beta\rangle$ has fidelity $F_\beta = |\langle\psi_i|\psi_\beta\rangle|^2 = [2+\cos\beta_1 - \cos\beta_2 + \cos(\beta_1+\beta_2+\beta_3) - \cos(\beta_1-\beta_2) - \cos(\beta_1+\beta_3) + \cos(\beta_2+\beta_3)]/8$ with the ideal state.

We use $\overline{\cdots}$ to denote the average over the fluctuations of the phases β_1, β_2, and β_3. Considering the control qubit in the absence of a target qubit, we obtain the output Stokes parameters $S_{H,\beta_1} = \cos\beta_1$, $S_{D,\beta_1} = \sin\beta_1$ and $S_{R,\beta_1} = 0$ for the input state vector $|H\rangle$ and a specific value of the random variable β_1. The ensemble averages are $S_H = \overline{S_{H,\beta_1}} = \overline{\cos\beta_1}$, $S_D = \overline{\sin\beta_1}$, and $S_R = 0$ so that the visibility is $V_c = V_1 = [(\overline{\sin\beta_1})^2 + (\overline{\cos\beta_1})^2]^{1/2}$. The fidelity between the single-qubit input state $|H\rangle$ and the single-qubit output state ρ_{out} is $F_1 = \langle H|\rho_{\text{out}}|H\rangle = (1+S_H)/2$. The average value $\overline{\beta_1}$ can be varied in the experiment. Assuming that V_1 remains unchanged when doing so, we obtain the maximum $F_{1,m} = \frac{1+V_1}{2}$. Likewise, considering only the target qubit in the absence of the control qubit, we obtain $V_2 = [(\overline{\sin\beta_2})^2 + (\overline{\cos\beta_2})^2]^{1/2}$ and $F_{2,m} = (1+V_2)/2$. In analogy to these expressions, we formally define $V_3 = [(\overline{\sin\beta_3})^2 + (\overline{\cos\beta_3})^2]^{1/2}$ and $F_{3,m} = (1+V_3)/2$.

We now turn to the entangling-gate operation. For the input state vector $|HH\rangle$, our model yields the output density matrix $\rho = \overline{|\psi_\beta\rangle\langle\psi_\beta|}$ and the fidelity $F_e = \langle\psi_i|\rho|\psi_i\rangle = \overline{F_\beta}$. To evaluate this expression, we use trigonometric identities such as $\cos(\beta_1+\beta_2) = \cos\beta_1\cos\beta_2 - \sin\beta_1\sin\beta_2$. For simplicity, we assume that the fluctuations in the variables β_1, β_2, and β_3 are uncorrelated. Hence, $\overline{\cos\beta_1\cos\beta_2} = \overline{\cos\beta_1}\;\overline{\cos\beta_2}$ etc. We assume that the average values $\overline{\beta_i}$ are chosen such that F_e is maximised at fixed values of V_1, V_2, and V_3. We also assume that the probability distribution function of each β_i is symmetric around its average value. Hence, F_e is maximised if we choose $\overline{\beta_1} = 0$ and $\overline{\beta_2} = \overline{\beta_3} = \pi$. This yields $\overline{\sin\beta_i} = 0$, $\overline{\cos\beta_1} = V_1$, $\overline{\cos\beta_2} = -V_2$, $\overline{\cos\beta_3} = -V_3$. A straightforward calculation now yields

$$F_e = \frac{1+V_1}{2}\,\frac{1+V_2}{2}\,\frac{1+V_3}{2} + \frac{1-V_3}{8}. \qquad \text{(S6)}$$

Using the same methods, we find that the visibility V_t measured in Ref. [1] in the presence of a stored $|L\rangle$ control excitation is $V_t = V_2V_3$. Given the measured value V_t but with unknown V_2 and V_3, the expression for F_e is maximised if we assume $V_2 = 1$ and $V_t = V_3$. As additional experimental imperfections tend to lower F_e even further, we obtain the upper bound $F_e \le (1+V_c)(1+V_t)/4 + (1-V_t)/8$. Using the value $V_c = 0.66(2)$ measured here and the value $V_t = 0.75(14)$ measured in Ref. [1], we obtain the upper bound $F_e \le 0.76(6)$. Several effects might contribute to the fact that the measured value of F_e does not reach this upper bound, e.g., events in which more than one control or more than one target photon impinge on the atomic sample (Methods), a possible reduction of the visibility of the control qubit resulting from the Rydberg interactions with the target photon, or imperfections in the experimental determination of the optimal mean values of the phases $\overline{\beta_j}$.

It is interesting to investigate whether the assumption that all imperfections are modelled as phase fluctuations has a large effect onto the resulting upper bound for F_e at given measured values of V_c and V_t. To address this question, we developed an analogous model that is based purely on population fluctuations. As long as all fluctuations are small, we find that the resulting upper bound is identical to the upper bound estimated from pure phase fluctuations. In the experiment both types of fluctuations exist. But as the investigation of both extreme cases — pure phase fluctuations or pure population fluctuations — predict identical upper bounds, it seems likely that a model taking both types of fluctuations into account simultaneously will predict a similar upper bound, as long as all fluctuations are small. This result is plausible because when taking only phase fluctuations into account, the amount of phase fluctuations needed to explain the observed values of V_c and V_t is larger than if both population and phase fluctuations are included in the model.

G. Comparison with a Phase Shift Induced by Excitation Hopping

A recent experiment [10] studied an alternative mechanism for creating a conditional phase shift of $\pi/2$. This prompts two questions. First, why does the mechanism studied there not occur in our experiment? Second, if we used that mechanism instead of ours would that improve the performance of the photon-photon gate?

To answer the first question, we note that the conditional phase shift in Ref. [10] is created as a result of excitation hopping between a propagating Rydberg polariton coupling to the $|100S\rangle$ state and a stored Rydberg excitation in the $|99P\rangle$ state. In principle, an analogous process could occur in our experiment with the states $|67S\rangle$ and $|69S\rangle$. But in practice, it is negligible for two reasons. First, both excitations in our experiment are in S states which makes hopping a much slower second-order process. Second, the states used in our experiment exhibit predominantly van der Waals interaction, not excitation hopping. To quantify this, the van der Waals interaction at distance r can be characterised by $V_b(r) = -C_6/r^6$ and the second-order excitation hopping by $V_{ex}(r) = -\chi_6/r^6$, see e.g. Ref. [10]. We use quantum defect theory to calculate $C_6/\chi_6 = 29$ for the states used in our experiment, which shows that the van der Waals interaction dominates.

To answer the second question, we compare the performance of the two systems. We first note that our present work goes far beyond the scope of Ref. [10] because we demonstrate a quantum gate, not just a conditional phase shift. When comparing experiments which create a conditional phase shift, such as Refs. [1] and [10], the crucial figures of merit are conditional phase shift, visibility, and efficiency.

In terms of the size of the conditional phase shift Ref. [10] was already outperformed by our previous work [1] where we demonstrated a conditional phase shift of π, not just $\pi/2$. In theory, any system creating a small conditional phase shift could be cascaded many times to eventually reach a π phase shift but in practice this is hardly ever done because it tends to cause severe setbacks in terms of visibility and efficiency. As a consequence, a phase shift of π has evolved into the standard benchmark because, first, creating an even larger phase shift is typically not helpful and, second, single-qubit unitaries provide an invertible map between a CNOT gate and a π phase gate, thus offering a simple possibility to compare with the performance of implementations of CNOT gates in completely different physical systems.

The role of the visibility in comparing systems which create conditional phase shifts is similar to the role of the post-selected fidelity in comparing quantum gates. It is a really crucial parameter that characterizes the degree of phase coherence in the system. In Ref. [1] we observed a visibility of 75(14)%. Unfortunately, the visibility seems to be missing completely in Ref. [10], making a comparison in terms of the visibility impossible.

Finally, the efficiency observed in Ref. [10] was $\eta = 0.06 \times 0.82 = 0.049$ for storage and retrieval of the first photon and $T = 0.56 \times 0.77 = 0.43$ for transmission of the second photon. To obtain a realistic comparison with our work, Ref. [10] would have to double its conditional phase shift. One could hypothesize that sending the second photon twice through the medium might double the conditional phase shift. Based on this one could optimistically extrapolate the total efficiency to be at best $0.82 \times 0.75\ T^2\eta = 0.0056$. The factor T^2 expresses the transmission after passing twice through the medium. The factor 0.82 describes the reduction of the retrieval efficiency because of Rydberg interactions during the second passage of the second photon. The factor 0.75 estimates the reduction of the retrieval efficiency expected from thermal atomic motion at a temperature of 20 μK because the dark time $t_d = 1.4\ \mu$s between storage and retrieval must be doubled. Taking only thermal motion into account, the retrieval efficiency is expected to decay according to (see e.g. Refs. [2, 11]) $e^{-(t_d/\tau)^2}$ where $\tau = \frac{\lambda_{dB}}{\sqrt{2\pi}v_r} = 4.5\ \mu$s is the $1/e$ time, λ_{dB} the thermal de Broglie wavelength, and v_r the relative speed between a ground-state atom and a Rydberg atom created by differential photon recoil during storage. Hence, doubling t_d yields a factor $e^{-(2t_d/\tau)^2}/e^{-(t_d/\tau)^2} = 0.75$. Of course, it is unpredictable whether the system studied in Ref. [10] will be able to reach the above extrapolation or whether additional experimental complications will occur. Anyway, this optimistic extrapolation would suggest that Ref. [10] and our work would perform almost identically in terms of efficiency.

[1] Tiarks, D., Schmidt, S., Rempe, G. & Dürr, S. Optical π phase shift created with a single-photon pulse. *Sci. Adv.* **2**, 1600036 (2016).

[2] Baur, S. E. *A Single-Photon Switch and Transistor Based on Rydberg Blockade*, PhD thesis, Technische Universität München (2014).

[3] Mirgorodskiy, I. *et al.* Electromagnetically induced transparency of ultra-long-range Rydberg molecules. *Phys. Rev. A* **96**, 011402 (2017).

[4] Fleischhauer, M., Imamoglu, A. & Marangos, J. P. Electromagnetically induced transparency: Optics in coherent media. *Rev. Mod. Phys.* **77**, 633–673 (2005).

[5] Tiarks, D., Baur, S., Schneider, K., Dürr, S. & Rempe, G. Single-photon transistor using a Förster resonance. *Phys. Rev. Lett.* **113**, 053602 (2014).

[6] Firstenberg, O. *et al.* Attractive photons in a quantum nonlinear medium. *Nature* **502**, 71–75 (2013).

[7] Hao, Y. M. *et al.* Quantum controlled-phase-flip gate between a flying optical photon and a Rydberg atomic ensemble. *Sci. Rep.* **5**, 10005 (2015).

[8] Das, S. *et al.* Photonic controlled-PHASE gates through Rydberg blockade in optical cavities. *Phys. Rev. A* **93**, 040303 (2016).

[9] Wade, A. C. J., Mattioli, M. & Mølmer, K. Single-atom single-photon coupling facilitated by atomic-ensemble dark-state mechanisms. *Phys. Rev. A* **94**, 053830 (2016).

[10] Thompson, J. D. *et al.* Symmetry-protected collisions between strongly interacting photons. *Nature* **542**, 206–209 (2017).

[11] Jenkins, S. D., Zhang, T. & Kennedy, T. A. B. Motional dephasing of atomic clock spin waves in an optical lattice. *J. Phys. B* **45**, 124005 (2012).